Thermal Effects in the Evolution of Initially Layered Mantle Material

Running Title: Thermal Effects in Layered Mantle Material

M Davies (Corresponding Author)
Earth Systems Science and Computational Centre (ESSCC),
The University of Queensland,
St Lucia QLD 4072,
Australia
matt@esscc.uq.edu.au

H Mühlhaus
Earth Systems Science and Computational Centre (ESSCC),
The University of Queensland,
St Lucia QLD 4072,
Australia
– and –
CSIRO Division of Exploration and Mining,
26 Dick Perry Ave,
Kensington WA 6051,
Australia
muhlhaus@esscc.uq.edu.au

L Gross
Earth Systems Science and Computational Centre (ESSCC),
The University of Queensland,
St Lucia QLD 4072,
Australia
gross@esscc.uq.edu.au

Thermal Effects in the Evolution of Initially Layered Mantle Material

M Davies, H Mühlhaus and L Gross

Abstract. A simplified model for anisotropic mantle convection based on a novel class of rheologies, originally developed for folding instabilities in multilayered rock [4], is extended through the introduction of a thermal anisotropy dependent on the local layering. To examine the effect of the thermal anisotropy on the evolution of mantle material, a parallel implementation of this model was undertaken using the *Escript* modelling toolkit and the *Finley* finite element computational kernel [3]. For the cases studied, there appears to little if any effect. For comparative purposes, the effects of anisotropic shear viscosity and the introduced thermal anisotropy are also presented. These results contribute to the characterisation of viscous anisotropic mantle convection subject to variation in thermal conductivities and shear viscosities.

Keywords. anisotropy, folding, alignment, mantle.

1. Introduction

The convection of the Earth's mantle is the underlying dynamic process that drives the motion of its lithospheric plates. The convection process, in turn, is a result of the gravitational instability of material within the mantle and its temperature-dependent density. As warmer buoyant material rises, it displaces colder, denser material that sinks. Conversely, as the warmer material rises, it cools, and, as the colder material sinks, it warms and increases its buoyancy. It is through this continuous pseudo-cyclic mechanism that currents are established within the Earth

that carry warmer material toward the surface, displacing cooler material to the interior.

The simulation of anisotropic mantle convection has been a specialized area where it is often assumed that the instantaneous flow patterns predicted by convection simulations could be directly related to seismic anisotropy. However, recent studies indicate that recorded observations diverge from this assumption and that the effect of anisotropic shearing is of a complex nature [6]. In response to these observations, a novel class of rheologies for folding instabilities in multilayered rock have been developed [4] and then later extended [5] to address feedback processes for large-scale flow where the effects of layer obstruction, misalignment and realignment are evident. The approach is unique in that the local material layering is treated as an independently evolving state of the convection process. This paper adopts this approach in a simple model to investigate the evolution of initially layered mantle material. The simple model is formulated here to include an anisotropic thermal conductivity.

2. The Model

The physics of mantle convection processes are typically modeled under the standard assumption that mantle material under large deformation can be compared to an incompressible, highly-viscous fluid. Based on this assumption, a viscous anisotropic mantle convection model has been developed for the study of deformation processes in multilayered geological formations. In terms of a nondimensionalised system, the general governing equations of mantle convection are given by the stress equilibrium equation and the heat conservation equation respectively:

$$\sigma'_{ij,j} - p^{\mathrm{th}}_{,i} + Ra^{\mathrm{c}} T z_i = 0 \tag{1}$$

$$\dot{T} = \left(K_{ij} T_{,j}\right)_{,i} + \frac{Di^{\mathrm{c}}}{Ra^{\mathrm{c}}} \sigma'_{ij} D_{ij} \tag{2}$$

where σ' is the deviatoric stress, p^{th} is the pressure due to thermal effects, T is the temperature, $\dot{T}$ denotes the material time derivative of the temperature, z_i is a unit vector in the opposite direction to gravity, K is the thermal conductivity tensor, Di^{c} is the computational dissipation number, Ra^{c} is the computational Rayleigh number and D is the stretching (deformation rate) tensor. As the mantle material is incompressible ($v_{i,i} = 0$), the Boussinesq approximation is adopted in the last term of (1). The Boussinesq approximation requires that the fluid bouancy is proportional to the fluid temperature in the convective system and is implemented as a linear density variation with temperature as given by:

$$\rho = \rho_0 \left(1 - \alpha (T - T_{\mathrm{c}})\right) \tag{3}$$

where α is the coefficient of thermal expansion relative to T_{c}, the temperature at the cold boundary. In equation (1) we assume $T_{\mathrm{c}} = 0$.

2.1. Anisotropic Model Refinements

An initially layered, transverse-isotropic, viscous mantle material which is heated from below is now considered. Such a material can represent an alternating sequence of composite heterogeneous layers of variable rheology or a weakly bonded sequence of homogeneous layers. After the onset of convection, the initially anisotropic layered mantle material mixes as it evolves. As a result, the anisotropic effects arising from the layer evolution change dynamically. In this paper we study the effects of viscous shearing with an introduced formulation for explicit thermal conductivity variations along a layer.

The anisotropic viscous shearing effect is characterised by two effective shear viscosities, denoted as η and η_S, where η_S is introduced as the shear viscosity

for flow along a layer. The shear stress arising from the deviatoric stretching is consequently corrected by the 4th order anisotropy tensor Λ (see [4] for details on the derivation of Λ) such that:

$$\sigma'_{ij} = 2\eta D'_{ij} + 2(\eta_S - \eta)\Lambda_{ijkl} D'_{kl} \tag{4}$$

where $\Lambda_{ijkl} = \frac{1}{2}\left(n_i n_k \delta_{lj} + n_j n_k \delta_{il} + n_i n_l \delta_{kj} + n_j n_l \delta_{ik}\right) - 2n_i n_j n_k n_l$ and n is a normal surface vector, or *"director",* defining the orientation of the material layering known.

In a similar manner, we introduce a thermal anisotropic effect, characterised by two thermal conductivities κ and κ_L, where κ_L is thermal conductivity along a layer. The thermal conductivity tensor K is then composed of an isotropic part and an anisotropic correction such that:

$$K_{ij} = \kappa_L \delta_{ij} + (\kappa - \kappa_L)\, n_i n_j \tag{5}$$

Effects such as anisotropic flow misalignment can be captured through the use of the director as a distinct material property. As the director transforms with a material surface element in a continuum, Nanson's relation [1] can be used to describe the evolution of the director with time as a both a translation and rotation with the velocity field. In turn, this relation can be simplified conditionally where the direction of the director is the only unknown:

$$\dot{n} = -v_{j,i} n_j \tag{6}$$

The use of this simplification requires that care is taken to ensure that the director retains unit length during computation. It is shown in [5] that viscous slip planes tend to align with velocity vectors in steady states, and subsequently that a solution to (6) is indeed flow-aligned at steady state.

3. Computational Strategy

The domain is a square 2-dimensional domain with the length of a side being equal to 1 (nondimensionalised), representative of an isolated region of the Earth's mantle. The base of the region is maintained at a constant temperature as it is heated from below. Similarly, the top surface of the region is a cold boundary that is also of constant temperature. There is no temperature change across the vertical surfaces. The velocity, v, director, n, and temperature, T, are independent variables that are solved sequentially at each time step of the simulation using the finite element method (FEM). As mentioned earlier, care is taken to ensure that the magnitude of the director is reset to unit length as soon as it is solved.

Substitution of (4) into (1) yields a second order linear equation for which the incompressible velocity, v, and the pressure due to thermal expansion, p^{th}, are unknown. Adopting a simple penalty method, a discretisation is derived for solution of v and p^{th}at time $t + \delta t$:

$$p^{th\,(\alpha+1)} = p^{th\,(\alpha)} - P v_{j,j}^{(t+\delta t)\,(\alpha)} \tag{7}$$

$$\Big[(\eta(\delta_{ik}\delta_{jl} + \delta_{il}\delta_{jk}) + 2(\eta_S - \eta)\Lambda_{ijkl}^{(t)} + P\delta_{ij}\delta_{kl})v_{k,l}^{(t+\delta t)\,(\alpha+1)}\Big]_{,j} - \Big[p^{\mathrm{th}\,(\alpha)}\delta_{ji}\Big]_{,j} + Ra^c T^{(t)} z_i = 0 \tag{8}$$

Here, $P \gg \eta$ is introduced as a penalty factor.

In a similar manner, the heat equation (2) and the director evolution equation (6) are discretised through the introduction of both a backward difference approximation for the time derivative and additional terms for upwinding (upwinding is discussed in section 3.2).

For unstructured meshes, a forward-centred time step δt^+ is determined from a first order implicit extrapolation based on the Courant condition. The scheme computes δt^+ from the average value of the maximum velocity predicted implicitly for the ensuing computation:

$$\delta t^+ = \frac{\sqrt{\delta t^- (\delta t^- v_{\max}^{(t)\,2} + 2(v_{\max}^{(t)} - v_{\max}^{(t-\delta t)})Ch)} - \delta t^- v_{\max}^{(t)}}{v_{\max}^{(t)} - v_{\max}^{(t-\delta t)}} \tag{9}$$

where C is an appropriate Courant number, h is the mesh discretisation scale, and $v_{\max}$ is the maximum magnitude of the nodal point velocities. Due to the adaptive nature of this extrapolation scheme, larger values of C can be trialed.

3.1. Implementation

The authors[1] have designed and developed a *Python* scripting language toolkit "*Escript*" to facilitate the simulation of solid Earth processes [3]. *Escript* provides a scripting interface to parallelised computational kernels in order to shield a modeller from developing low-level parallelism constructs. For the results of this paper, the "*Finley*" FEM computational kernel is used to implement the finite element method to solve the velocity, director and temperature equations. A brief overview of *Escript*, *Finley* and the FEM implementation is presented in this section.

3.1.1. Escript. At the core of *Escript* is the *Data* module. *Data* is semantically associated with an arbitrary computational domain or distribution which is implemented or managed through a computational kernel interface. Through the provision of a standard interface, the *Data* module provides the means to exchange data between various kernels while maintaining full contextual information in regard to

[1]The *Escript* and *Finley* projects at ESSCC are led by Lutz Gross.

its source and intended use. *Data* objects may be scalars, vectors, or tensors of up to 4th order.

The association of domain information with *Data* objects enables an implicit form of domain-based parallelism. As an example, the *Data* object expression `C=A+B`, where `C`, `A` and `B` are associated with the nodes of a FEM mesh, executes an addition in parallel. Composite numerical methods such as specialised nonlinear solvers and time-differencing schemes can be rapidly developed using a compact high-level domain-wide syntax with a simple implicit parallelism.

3.1.2. Finley. To use *Finley*, *Data* expressions are used to transform an initial boundary value problem (IBVP) into a sequence of linear boundary value problems (BVPs) to be solved at each time step. Each linear BVP can then be provided to *Finley* to assemble a stiffness matrix using a discretisation based on the standard variational formulation [7]. The discretisation is appropriate for the mesh and element type.

For an unknown vector function u, the partial differential equations (PDEs) of a BVP (eg (8), (6)) are provided to *Finley* through the specification of the coefficients of the following templated form in tensorial notation:

$$-(A_{ijkl}u_{k,l})_{,j} - (B_{ijk}u_k)_{,j} + C_{ikl}u_{k,l} + D_{ik}u_k = -X_{ij,j} + Y_i \qquad (10)$$

The tensorial coefficients A, B, C, D, X and Y are functions of their location in the physical domain and are supplied to *Finley* as *Data* objects or expressions. For example, to solve the velocity equation (8), a simple rearrangement into a form comparable with (10) determines that it is necessary only to provide *Finley* with A, X, and Y as *Data* objects or expressions. On the other hand, it is necessary to

provide *Finley* with all of the coefficients[2] to solve the director evolution equation (6) after introducing the required upwinding terms.

To complete the BVP, *Finley* also provides forms for both Neumann and Dirichlet boundary conditions as given by the respective systems:

$$n_j(A_{ijkl}u_{k,l} + B_{ijk}u_k) + d_{ik}u_k = n_jX_{ij} + y_i \text{ on } \Gamma^N \tag{11}$$

$$u_i = r_i \text{ on } \Gamma^D \tag{12}$$

where n denotes the outer boundary normal, and A, B and X are as previously defined. Here, d and y are coefficients defined on the natural boundary Γ^N while r is a function defined on the Dirichlet boundary Γ^D. The complete linear BVP for systems of equations is then defined by (10)–(12). *Finley* also defines a steady BVP for a single equation in a scalar unknown.

3.2. Upwinding

Both the hyperbolic director evolution equation (6) and the parabolic heat equation (2) are advection dominated at high Rayleigh numbers. To avoid the spurious oscillations that would otherwise arise during the computation of their solution, it is necessary to introduce an upwinding scheme to their discretisation. The *de facto* standard upwinding scheme is the streamline upwind Petrov-Galerkin (SUPG) method [7], which implements a modification to the weight functions of the FEM formulation. However, as *Finley* does not permit the direct manipulation of the FEM assembly process, it is not possible to use this scheme. To address this issue, a modified PDE is derived in-place. This modified PDE is based on the original PDE and includes additional terms that eliminate the most significant advective

[2]As per section 3.2, the coefficients (being like terms) of a modified equation are provided to *Finley* in this case.

truncation error terms for an explicit discretisation[3]. For a general first order differential expression $Lu = au + bu_{,i}v_i + c$, the modified operator is given by:

$$L \longleftarrow L - (L\beta_i)_{,i} \tag{13}$$

where $\beta_i = \frac{h}{2}\frac{v_i}{\sqrt{v_j v_j}}$. For pure advection problems with regular quadrilateral mesh elements, this approach is equivalent to the SUPG method. The strategy of this approach can be compared to that of the Taylor-Galerkin upwinding scheme described in [7].

4. Results and Discussion

Simulations have been run for a range of thermal and viscous anisotropies. The simulations are based on 50×50 square meshes of bilinear quadrilateral finite elements. The system is at rest initially with an initial layering perpendicular to the direction of depth and an initial temperature perturbation is given by:

$$T = 1 + \frac{1}{10}cos(\pi x_1)sin(\pi x_2) - x_2 \tag{14}$$

A parameter space of $\eta_S/\eta = \{0.1, 0.5, 1.0\}$ against $\kappa_L/\kappa = \{0.9, 1.0, 1.1\}$ for $Ra^c = 10^5$ and $Di^c = 0$ was studied. A comparison of Nusselt number plots and maximum shear stresses is shown in figure (1). The Nusselt number derived for the purpose of characterising the resultant convection profiles is expressed in terms of the mechanical power:

$$Nu = 1 - \frac{1}{Ra^c}\frac{\int_V v_{i,j}\sigma_{ij}dV}{\int_V K_{ij}T_{,j}z_i dV} \tag{15}$$

[3]This approach is commonly applied in the finite difference method.

A comparison of these plots illustrates that the thermal conductivity effects add an additional wavelength to the Nusselt number which appears to dampen with time. The effects also appear to have little effect on the maximum shear profile and despite the additional damping wavelength, the average Nusselt number is unchanged. It has been proposed by Christensen [2], that the Nusselt number for an anisotropic convection process can be compared to the Nusselt number of an isotropic convection process with average viscosity $(\eta + \eta_S)/2$. Such a comparison has been made in figure (2) . While the Nusselt number of the isotropic process exceeds marginally the running average of the original anisotropic process, it does maintain a comparable trajectory.

A comparison of the temperature field and isotherms is shown in figure (3) at $t = 0.2$ for $Ra^c = 10^5$. It is shown that there are but subtle differences in the anisotropic temperature profiles (b), (c) and (d). A comparison of sub-figures (b) and (c) demonstrate that for $\kappa_L/\kappa = 1.1$ there is a subtle increase in the thermal gradient at the cell boundaries. Conversely, a comparison of sub-figures (b) and (d) demonstrate that for $\kappa_L/\kappa = 0.9$ there is a subtle decrease in the thermal gradient at the cell boundaries.

A comparison of the streamlines, velocity and the nonalignment field is shown in figure (4) at $t = 0.2$ for $Ra^c = 10^5$. The nonalignment field is measured by the function $N = abs(n_i v_i/\sqrt{v_k v_k})$. While both isotropic and anisotropic convection has been reported to produce cells that encompass a mechanically-stagnant core [5], the results obtained for this study evidenced subtle periodic adjustments in the core position. Feedback processes of anisotropic systems appear to result in a higher degree of mixing and episodic periods of misalignment in comparison with the corresponding isotropic system. The range of simulations performed evidenced that large fluctuations in the degree of alignment were spasmodic and perhaps

oscillatory. The degree of oscillation evident in the convection process for long running simulations with anisotropic shear viscosity questions the existence of a true steady state in this computational scheme.

It can be argued that the irregular oscillatory nature of the convection system as a result of anisotropic shear viscosity is both a result of feedback processes and a potential artifact of computation involving spurious discontinuities arising in director interpolation. There are two observations in support of this: (1) it has been demonstrated that the degree of oscillation decreases with mesh element size (particularly observable for $Ra^c = 10^6$); (2) the interaction of opposing directors for similarly-aligned folding layers at a displacement less than or equal to the mesh element size is left untreated. The first observation reflects the fact that the interpolation of directors in regions of high velocity gradient is inaccurate. The second observation reflects the need for further modeling and a more effective computational treatment. A potential solution to this problem in-part would be to evolve the directors' rotational orientation instead of their vector representation.

5. Conclusion

A simple model has been presented to investigate thermal conductivity effects in the evolution of initially layered material. For the presented case studies, it has been demonstrated that the evolution of anisotropic thermal conductivity effects on once-layered mantle material appears only to have a subtle influence on the resultant temperature gradients and velocity streamlines as steady state is approached.

Further simulation in the study of both larger 2-dimensional and 3-dimensional domains is likely to provide a better illustration of the variation in thermal convection patterns for thermal variation. Finally it is noted that the computational

treatment of the evolution of internal fluid surfaces in geodynamics remains a significant challenge at this time.

References

[1] Belytschko, T., Liu, W. K. and Moran, B., *Nonlinear finite elements for continua and structures* (John Wiley and Sons, 2001).

[2] Christensen, U. R. (1987), *Some geodynamical effects of anisotropic viscosity*, Geophys. J. R. Astr. Soc. 91, 711–736.

[3] Davies, M., Gross, L. and Mühlhaus, H. -B. (2004), *Scripting high performance earth systems simulations on the sgi altix 3700*, In Proceedings of the 7th international conference on high performance computing and grid in the asia pacific region, pp 244–251.

[4] Mühlhaus, H. -B., Moresi, L., Hobbs, B. and Dufour, F. (2002), *Large amplitude folding in finely layered viscoelastic rock structures*, Pure Appl. Geophys. 159, 2311–2333.

[5] Mühlhaus, H. -B., Moresi, L., and Čada, M. (2004), *Emergent anisotropy and flow alignment in viscous rock*, Pure Appl. Geophys. 161, 2451–2463.

[6] Simons, F. J., van der Hilst, R. D., Montagner, J. P. and Zielhuis, A. (2002), *Multimode rayleigh wave inversion for heterogeneity and azimuthal anisotropy of the australian upper mantle*, Geophysical J. Int. 151, 738–754.

[7] Zienkiewicz, O. C. and Taylor, R. L., *The finite element method* (Butterworth Heinemann, 2000), 5th ed., vol. 3.

Acknowledgment

This work has been supported by the Australian Computational Earth Systems Simulator Major National Research Facility (ACcESS MNRF), the Queensland

State Government, the University of Queensland and SGI. The Australian Commonwealth Government, participating institutions and both the Victorian and Western Australian State Governments fund the ACcESS MNRF.

M Davies
Earth Systems Science and Computational Centre (ESSCC),
The University of Queensland,
St Lucia QLD 4072,
Australia
e-mail: matt@esscc.uq.edu.au

H Mühlhaus
Earth Systems Science and Computational Centre (ESSCC),
The University of Queensland,
St Lucia QLD 4072,
Australia
– and –
CSIRO Division of Exploration and Mining,
26 Dick Perry Ave,
Kensington WA 6051,
Australia
e-mail: muhlhaus@esscc.uq.edu.au

L Gross
Earth Systems Science and Computational Centre (ESSCC),
The University of Queensland,
St Lucia QLD 4072,
Australia
e-mail: gross@esscc.uq.edu.au

Figure Captions

Figure 1. A comparison of Nusselt numbers for $Ra^{\mathrm{c}} = 10^5$and maximum shear stresses ($max(\sqrt{\sigma_{ij}\Lambda_{ijkl}\sigma_{kl}})$) along the layers.

Figure 2. A comparison between the Nusselt plots of an anisotropic convection process and a similar but isotropic ($\eta_S/\eta = 1$) convection process.

Figure 3. A comparison of temperature fields and isotherms at $t = 0.2$ for $Ra^{\mathrm{c}} = 10^5$. Subfigure (a) depicts the isotropic case.

Figure 4. A comparison of streamlines, velocity and nonalignment fields at $t = 0.2$ for $Ra^{\mathrm{c}} = 10^5$. Subfigure (a) depicts the isotropic case.

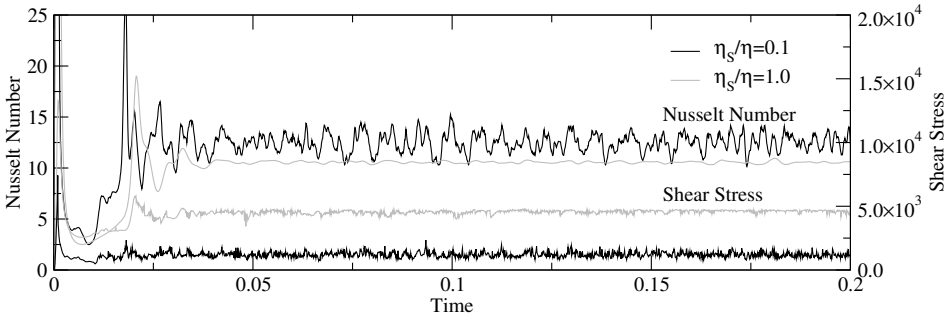

(a) $\kappa_L/\kappa = 0.9$.

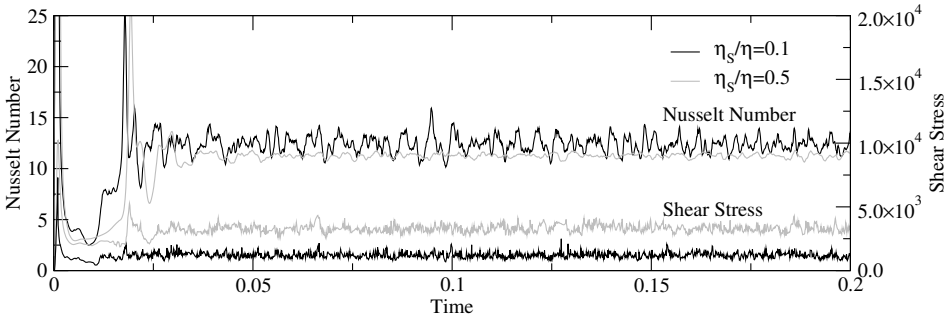

(b) $\kappa_L/\kappa = 1.0$.

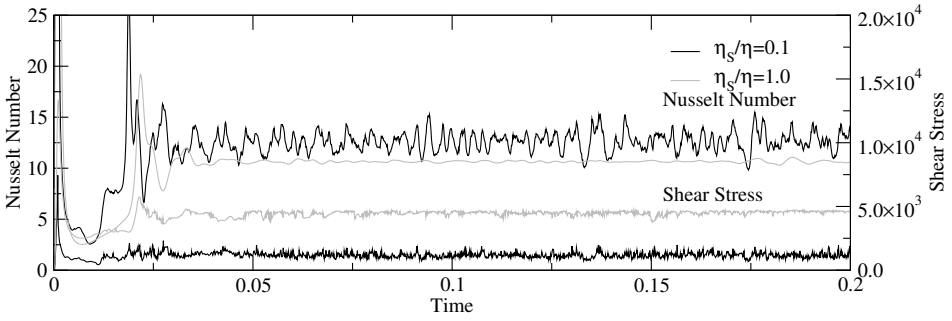

(c) $\kappa_L/\kappa = 1.1$.

FIGURE 1. A comparison of Nusselt numbers for $Ra^c = 10^5$and maximum shear stresses ($max(\sqrt{\sigma_{ij}\Lambda_{ijkl}\sigma_{kl}})$) along the layers.

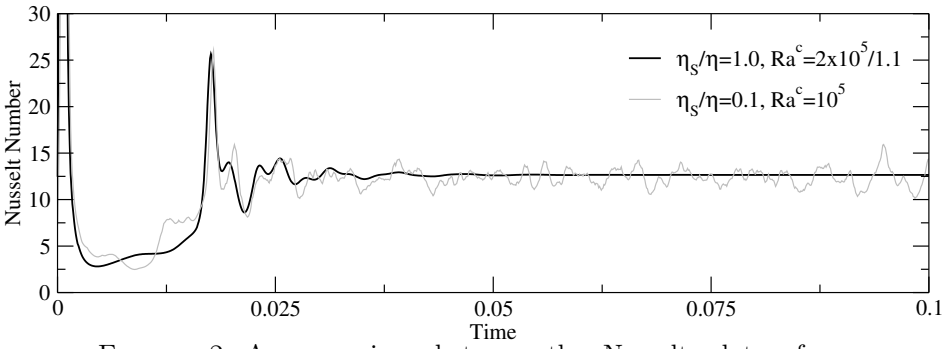

FIGURE 2. A comparison between the Nusselt plots of an anisotropic convection process and a similar but isotropic ($\eta_S/\eta = 1$) convection process.

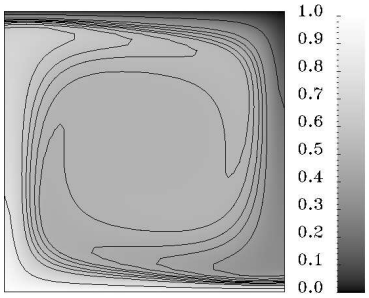

(a) $\kappa_L/\kappa = 1.0$, $\eta_S/\eta = 1.0$.

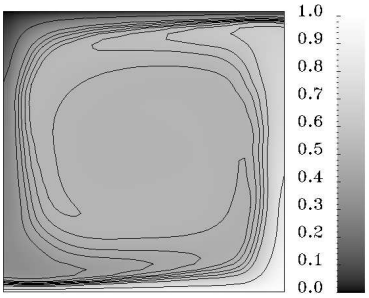

(b) $\kappa_L/\kappa = 1.0$, $\eta_S/\eta = 0.1$.

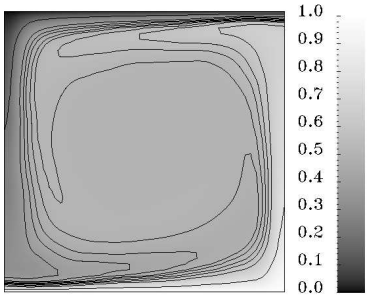

(c) $\kappa_L/\kappa = 1.1$, $\eta_S/\eta = 0.1$.

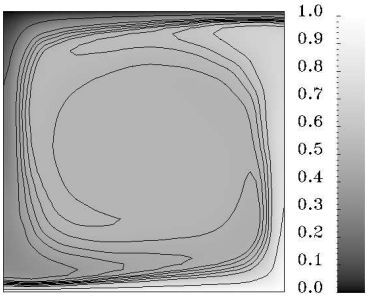

(d) $\kappa_L/\kappa = 0.9$, $\eta_S/\eta = 0.1$.

FIGURE 3. A comparison of temperature fields and isotherms at $t = 0.2$ for $Ra^c = 10^5$. Subfigure (a) depicts the isotropic case.

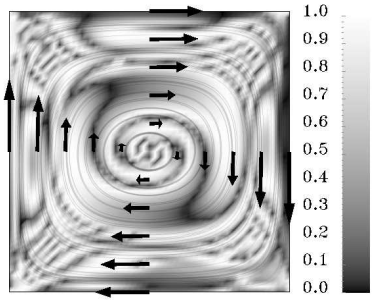

(a) $\kappa_L/\kappa = 1.0$, $\eta_S/\eta = 1.0$.

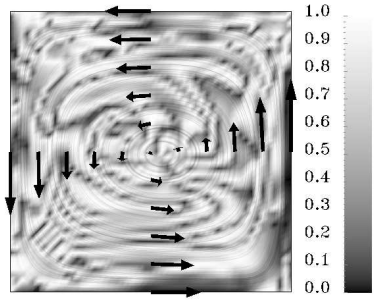

(b) $\kappa_L/\kappa = 1.0$, $\eta_S/\eta = 0.1$.

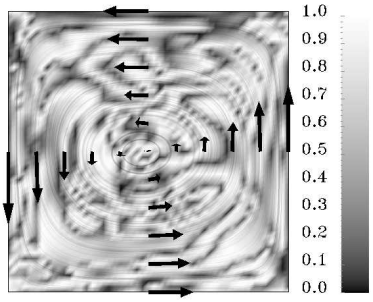

(c) $\kappa_L/\kappa = 1.1$, $\eta_S/\eta = 0.1$.

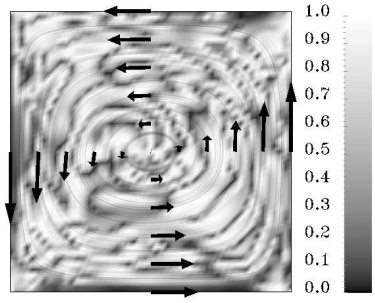

(d) $\kappa_L/\kappa = 0.9$, $\eta_S/\eta = 0.1$.

FIGURE 4. A comparison of streamlines, velocity and nonalignment fields at $t = 0.2$ for $Ra^c = 10^5$. Subfigure (a) depicts the isotropic case.